CONF-891119--6

DE90 003065

STRUCTURE OF AMORPHOUS Al_2O_3 PRODUCED BY ION IMPLANTATION

C. J. MCHARGUE, P. S. SKLAD, P. ANGELINI, C. W. WHITE, and J. C. MCCALLUM, OAK RIDGE NATIONAL LABORATORY, Oak Ridge, TN 37831-6118 USA and
A. PEREZ and G. MAREST, Univeristy Claude Bernard-Lyon 1, Villeurbanne, France

ABSTRACT

The amorphous state can be produced in α-Al_2O_3 by ion beam induced displacements at 77 K or by displacements combined with chemical effects at room temperature. Progress toward understanding the amorphization process has been made from studies of the short-range order, electronic charge on implanted species, and the critical composition for amorphization. Results are presented for implantation of Al + O in the stoichiometric ratio, zirconium, iron, and tin.

INTRODUCTION

From the earliest studies of ion implantation into Al_2O_3, there have been conflicting reports of amorphization. An understanding of the phenomenon is beginning to emerge from current studies of metal ion implantation to various fluences and at various substrate temperatures, and with the use of several techniques to characterize the resulting structures. It now appears that displacements alone can produce the amorphous state if the temperature is low enough to suppress dynamic recovery, but that "chemical effects" are important for many implanted species.

Implantation at low substrate temperatures (<100 K) will produce the amorphous state by damage accumulation alone at relatively low values of deposited damage energy [1]. The random value of backscattered yield in RBS spectra is reached at 0.3 keV/atom (2×10^{15} ion/cm^2) for 260 keV Cr-implantation at 77 K (c-axis orientation). Transmission electron microscopy and selected area electron diffraction patterns confirm the amorphous nature of the implanted zone. That the amorphization is due to damage accumulation and not to impurity effects was confirmed by stoichiometric implants of aluminum and oxygen.

In many instances, amorphization by room temperature implantation appears to be due to as yet unidentified "chemical effects". For example, implanting ^{90}Zr and ^{93}Nb to the same fluence at similar ion beam energies give different amounts of disorder with the former species producing an amorphous layer [2]. Since these implanted ions differ by only three atomic mass units, the details of the cascade formation should be similar, and differences in resultant disorder must originate in some chemical effect occurring during the post-cascade cool-down period.

Information about the structure of amorphous phases is generally limited since most characterization techniques provide only qualitative information.

Extended energy loss fine structure (EXELFS) analysis is sensitive to both structure and composition within near-neighbor distances of specific types of atoms in both crystalline and amorphous materials. The fine structure, which appears in the form of modulations on the core loss edges of electron energy loss spectra, results from diffraction of ejected core electrons by neighboring atoms. The ability to obtain EXELFS measurements with an analytical electron microscope allows direct observation of changes in composition, microstructure, and local atomic environment at a spatial resolution not attainable by other techniques. This procedure has been used to obtain modified radial distribution functions for Al_2O_3 amorphized at 77 K by implants of both Fe and stoichiometric (Al + O).

The Mössbauer effect provides a unique probe for investigating the structural aspects of solids on the atomic scale. Measurements of the hyperfine interactions provide information on symmetry, ordering, and chemical bonding in the immediate environment of the probed nucleus. Conversion electron Mössbauer spectroscopy (CEMS) is particularly suited for probing the near-surface region to a depth typical of the range of implanted ions. Studies that use CEMS in conjunction with Rutherford backscattering-ion channeling (RBS-C) and transmission electron microscopy (TEM) provide important information about the defect structure of implanted materials.

This paper will summarize recent information on the evidence for a critical composition for amorphization, the nature of short-range order in the amorphous state, and the chemical state of implanted species in amorphous Al_2O_3 produced by ion implantation.

EXPERIMENTAL PROCEDURES

High purity Al_2O_3 single crystals having the <0001> (c-axis) oriented normal to the surface were polished to an optical grade finish and were then annealed for 120 h at 1450°C in flowing O_2 to remove any residual polishing damage. The crystals were implanted with substrate temperatures of 77 K or 300 K using mass-analyzed beams of zirconium, iron, tin, or aluminum plus oxygen ions.

Rutherford backscattering and ion channeling measurements were performed with a beam of 2.0 MeV He^{++} at near-normal incidence to the sample surface and scattered into a surface-barrier detector at 160°. Ion channeling measurements were made with the beam aligned along the <0001> axis of the crystal.

Specimens for transmission microscopy were prepared in both cross-section and back-thinned geometries by mechanical polishing followed by ion milling. Analytical electron microscopy (AEM) was performed with either a Philips CM12 operating at 120 keV or a Philips EM400T/FEG operating at 100 keV. All EXELFS measurements were obtained at 300 kV with the use of a Philips EM430T equipped with an EDAX 9100/70 x-ray energy dispersive spectroscopy system and a Gatan 607 electron energy loss spectroscopy system. For each specimen examined, energy loss spectra were recorded for both the O K edge and the Al K edge by making multiple scans over the energy range desired while operating in the pulse mode. The spectra were recorded in the image mode (diffraction coupled). All spectra were deconvoluted prior to analysis. In order to avoid beam damage to the amorphous material, care was taken not to focus the beam during data collection and a liquid-nitrogen-cooled specimen holder was used.

Mössbauer spectra were obtained using the technique of CEMS. Two important features of CEMS for studies of implanted Al_2O_3 are: (1) CEMS probes only the surface to a depth of 150 to 200 nm, a thickness comparable to the depth of the implanted zone; and (2) aluminum and oxygen produce low photoelectron backgrounds in conversion-electron detection, thus yielding a high signal-to-noise ratio for the implanted iron.

In the present study, CEMS spectra were determined at room temperature using the backscattered geometry. The ^{57}Co source (100 mCi) was contained in a rhodium matrix and was mounted on a constant acceleration triangular-motion velocity transducer. The data were folded to produce a constant background. The velocity scale and all data are relative to a metallic α-iron absorber at room temperature. The Mössbauer spectra were fitted to Lorentzian line shapes with a computer least-squares procedure.

DISCUSSION OF RESULTS

Evidence for Critical Composition for Amorphization

The microstructure of a specimen implanted at 300 K with 175 keV zirconium ions to a fluence of 4×10^{16} ions/cm^2 is shown in Fig. 1. Electron microdiffraction revealed the presence of an amorphous layer located between two damaged but crystalline α-Al_2O_3 regions. The zirconium concentration profile in this specimen was determined from x-ray EDS line scans. The results presented in Fig. 2(a) show that the position of the subsurface amorphous layer as measured by TEM is centered on the experimentally measured zirconium depth profile which exhibits a maximum value of Zr/Al atom fraction of ≈0.13. The depth at which the amorphous layer starts, ≈40 nm, corresponds to a Zr/Al atomic fraction of approximately 0.08. The depth at which the amorphous layer ends, ≈95 nm, corresponds to a Zr/Al atomic fraction of ≈0.06. The interface between crystalline and amorphous alumina is irregular. The midpoint of the amorphous layer, ≈70 nm from the specimen surface, as determined from the image, corresponds very well with the depth at which the maximum in the measured zirconium depth profile occurs, ≈67 nm. These observations suggest there is a critical Zr/Al concentration above which the substrate becomes amorphous. The critical Zr/Al atomic fraction concentration level for these experiments is 0.065 ± 0.01.

Similar measurements were made on a specimen implanted under the same conditions but to a lower fluence of 2×10^{16} Zr/cm^2, Fig. 2(b). The subsurface amorphous region in this case extended from about 55 to 80 nm below the surface. The measured Zr/Al ratio at each position was 0.06 and the peak concentration (Zr/Al) was 0.075. There was no buried amorphous layer in a specimen implanted to 0.5×10^{16} Zr/cm^2.

These microstructural observations were compared to calculations of the rate of deposited energy as determined with both EDEP and TRIM computer codes. The position of the amorphous layer does not correspond to the displacement damage profile, but is closely related to the implanted species concentration profile. The peak in the calculated rate of energy deposition profile occurs closer to the surface than the peak of the implanted species depth profile. If the condition to amorphize the substrate were related to the displacement damage profile, the amorphous region would be located much closer to the surface than experimentally determined in the present study. The condition of a critical displacement damage level would locate the subsurface amorphous layer at depths between the surface and ≈30 nm rather than the observed position of between ≈45 and ≈90 nm.

Short-Range Order

The oxygen K edges obtained from EELS measurements of crystalline α-Al_2O_3 and the amorphous Al_2O_3 produced by a stoichiometric implant of Al (2×10^{16} ions/cm^2, 90 keV) and oxygen (3×10^{16} ions/cm^2, 55 keV) at 77 K are shown in Fig. 3. Differences in the shape and position of some of the oscillations are apparent. Data for the aluminum K edges exhibit similar differences. The oscillation function, $\chi(E)$, was isolated from the edge intensity by fitting a smooth function through the data. For the examples discussed here, a fourth-order polynomial fit provides the most reliable results [3].

Partial radial distribution functions were obtained in this manner for crystalline α-Al_2O_3, crystalline γ-Al_2O_3; an amorphous sample produced by a stoichiometric implant as above; and an amorphous sample produced by implantation of Fe (4×10^{16} ions/cm^2, 160 keV) at 77 K. These RDFs are given in Fig. 4 and show the Al-O first near-neighbor distances. The measured Al-O distances in the α-Al_2O_3 and the amorphous Fe-implanted Al_2O_3 have the same value, 0.185 nm, and the measured value agrees well with that calculated from the lattice constants. Similarly, the Al-O distances measured for the

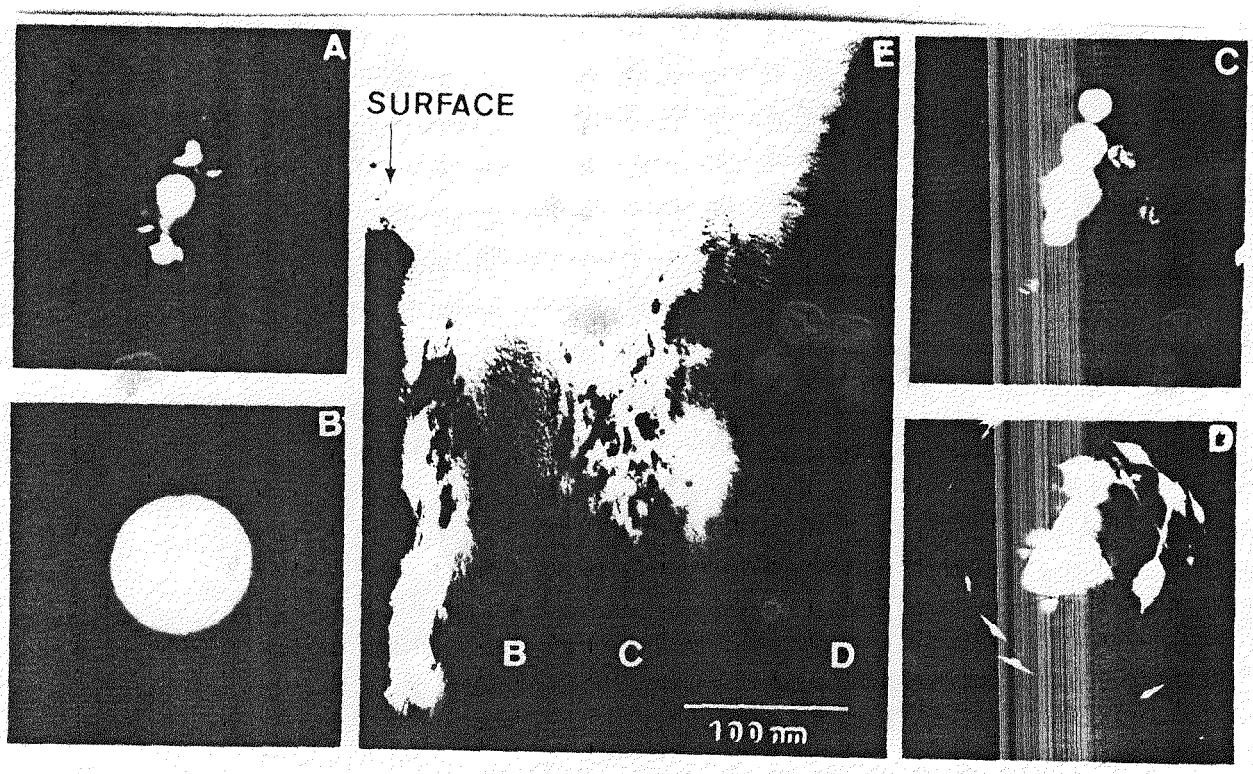

Fig. 1. Transmission electron micrograph of cross-sectioned sample of α-Al_2O_3 implanted with 4 x 10^{16} Zr/cm^2 (175 keV, 300 K). The selected area diffraction patterns indicate a buried amorphous layer.

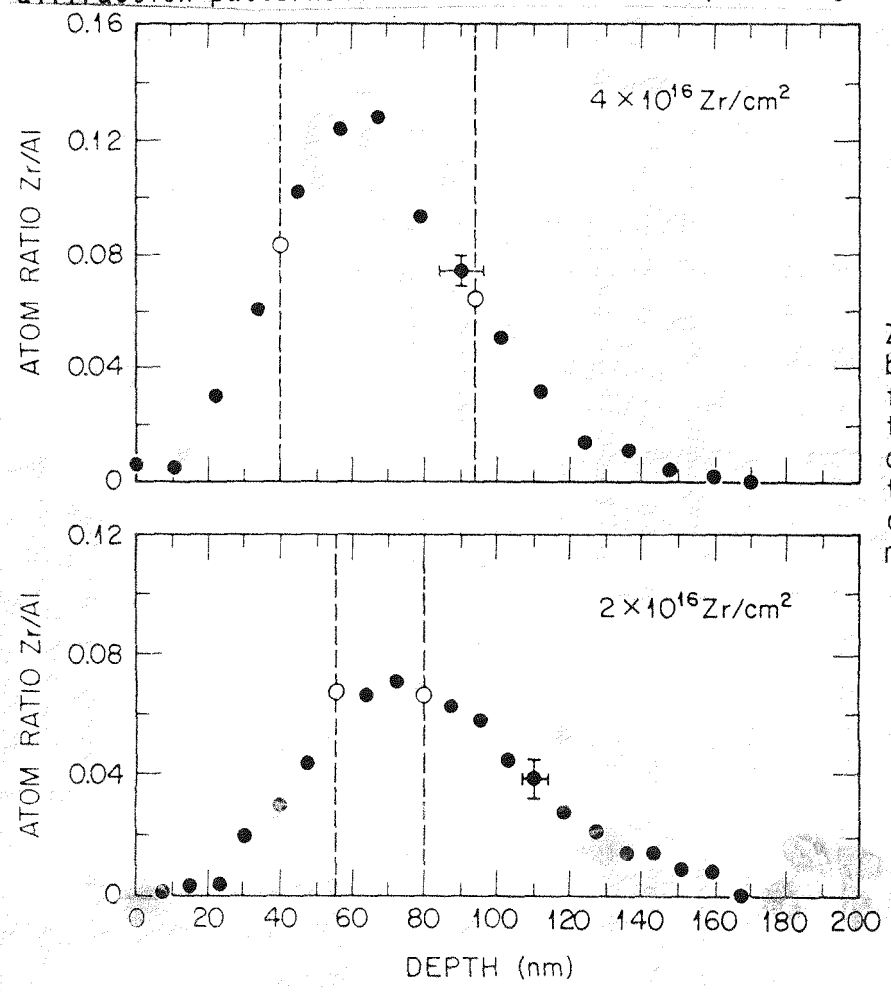

Fig. 2. The Zr/Al ratio determined by AEM is plotted as a function of depth from the surface. Vertical dotted lines correspond to position of amorphous/crystalline interface measured by TEM.

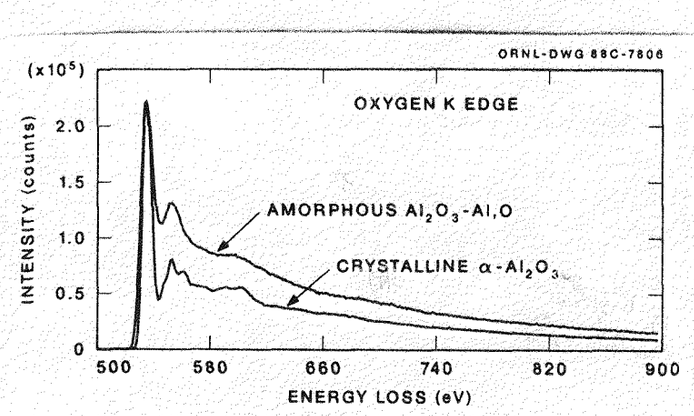

Fig. 3. Oxygen K edges from crystalline α-Al_2O_3 and amorphous stoichiometric-implanted Al_2O_3. The background has been subtracted.

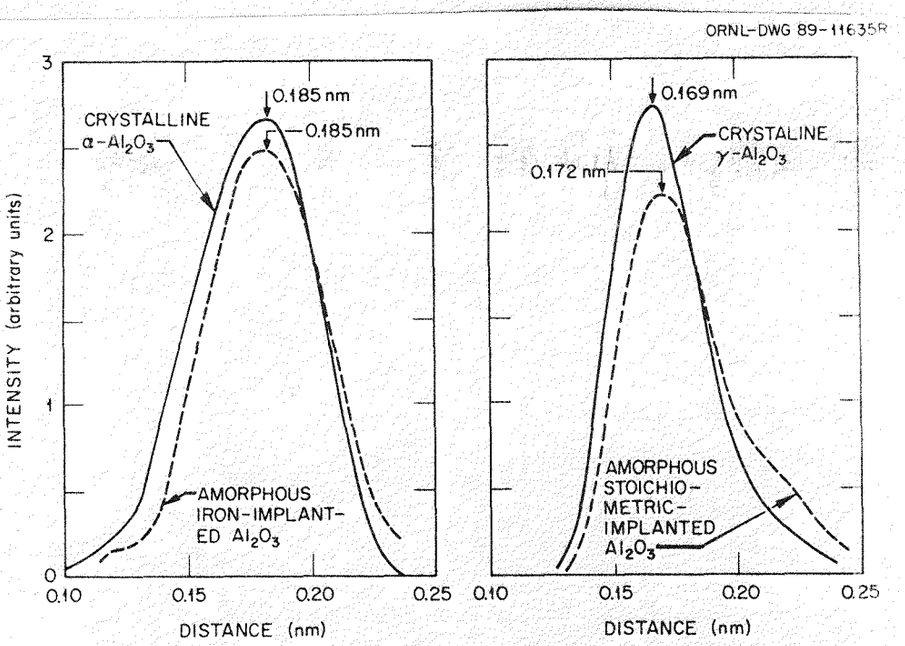

Fig. 4. Partial radial distribution functions determined from extended energy loss fine structure analysis (EXELFS).

γ-Al_2O_3 and the amorphous stoichiometric-implanted samples have smaller, but similar values, 0.169 and 0.172 nm, respectively.

The results of the EXELFS analysis clearly indicate the presence of short-range order in the amorphous Al_2O_3 produced by ion implantation at 77 K and, moreover, indicate that the nature of the short-range order is implantation species dependent.

Chemical State of Implanted Cations

Mössbauer spectra were determined for specimens implanted with ^{57}Fe (160 keV) at 77 K to fluences of 1, 2, 4, 7, and 10 x 10^{16} ions/cm^2 [4] and for a specimen implanted with ^{119}Sn (180 keV) at 300 K [5]. In each instance RBS/ion channeling and TEM showed the implanted region to be amorphous. The fact that implantation of tin at room temperature produces an amorphous state is additional evidence for a chemical effect.

The CEMS spectra measured at RT for samples implanted with 1,2,7, and 10 x 10^{16} Fe/cm^2 at 77 K are given in Fig. 5. A consistent fit to the spectra was obtained using four doublets and one single line, whose relative amounts varied with fluence. The single line was ascribed to small metallic iron clusters (Fe0). This line exhibits a negative IS (relative to bulk α-Fe) indicating that the clusters either are γ-Fe or are α-Fe under compression. The clusters in these amorphous matrices have not yet been detected in the electron microscope and no conclusion can be reached regarding their structure. Similar clusters, seen in Al_2O_3 implanted with 1 x 10^{17} Fe/cm^2 at 300 K have been identified in α-Fe.

Two quadrupole doublets were assigned to two different Fe^{2+} states. In the crystalline Fe-implanted Al_2O_3 one Fe^{2+} component was ascribed to a FeO (wustite)-type bond. However, the IS values for the Fe^{2+} component in the amorphous Fe-implanted Al_2O_3 are consistently higher and the QS values lower than those for FeO [6] or our earlier results [7] leading to an uncertainty in its nature. The parameters for the other Fe^{2+} are consistent with a $FeAl_2O_4$ spinel-type bond [8] as in the crystalline case. Further TEM and Mössbauer studies will be required in order to complete the description of the local environments and bonding for the Fe^{2+} components.

The other two doublets were assigned to two Fe^{4+} states with high spin configurations. This unusual oxidation state has been observed in nonstoichiometric perovskite-related compounds [9] where the Fe^{4+} occupies a tetragonally-distorted octahedral environment. This distortion, an elongation of the FeO_6 octahedron in one direction induces the high spin Fe^{4+} configuration. Such an elongation can be produced by increasing the covalency of the M-O bonds in the xy planes or from the presence of an oxygen vacancy in the octahedron. The two doublets for Fe^{4+} in our samples indicate the presence of two slightly different iron environments. In the present case, the Fe^{4+} ions are in an amorphous phase but we might suppose that the local order consists of distorted $Fe^{4+}O^6$ octahedra that contain oxygen vacancies or non-bridging oxygen ions.

The RBS/ion channeling spectra for Al_2O_3 implanted with 4 x 10^{16} Sn/cm^2 (180 keV, RT) show the aligned spectrum to reach the random value over a depth of about 70 to 80 nm, suggesting the presence of an amorphous layer. The amorphous nature of this region was confirmed by TEM observations. While the surface layer exhibited no coherently diffracting regions, the bright-field image does exhibit regions of varying contrast, suggesting compositional variations.

The CEMS spectra obtained for the Al_2O_3 samples implanted at room temperature with ^{119}Sn are given in Fig. 6. The spectra can be decomposed into two asymmetrical doublets having wide lines that can be attributed to Sn(II) and Sn(IV). The Mössbauer parameters suggest that the tin atoms are contained in local environments similar to those in compounds. In the absence of definitive electron diffraction results, we cannot specify the nature of this environment; e.g., whether there are small regions of SnO or only "SnO-like" bonding of the Sn.

Our results for the Sn(II) component (IS = 3.2 mm/s, QS = 2.1 mm/s, W = 1.3 mm/s) appear to favor a $SnAl_2O_4$ environment rather than SnO. The values of QS and W for the Sn(IV) component are comparable to those of SnO_2 or $SnAl_2O_5$ but the IS values are systematically negative and lower than the IS for these compounds. The TEM results suggest that the Sn-containing regions are amorphous. The lower IS values can be due to: (i) a higher ionicity of the Sn-O bonding in an amorphous Al_2O_3 matrix compared to that in SnO_2 or $SnAl_2O_5$; or (ii) a decrease in the electron density at the Sn nucleus due to a lower pressure exerted by the amorphous Al_2O_3 matrix on small precipitates.

The fact that both Sn(IV) and Fe(IV) have been observed in amorphous implanted Al_2O_3 leads to the speculation that this charge state may play an important role in the amorphization process. Crystalline SnO_2 has a rutile-type structure wherein the Sn^{4+} is located in a distorted octahedron of

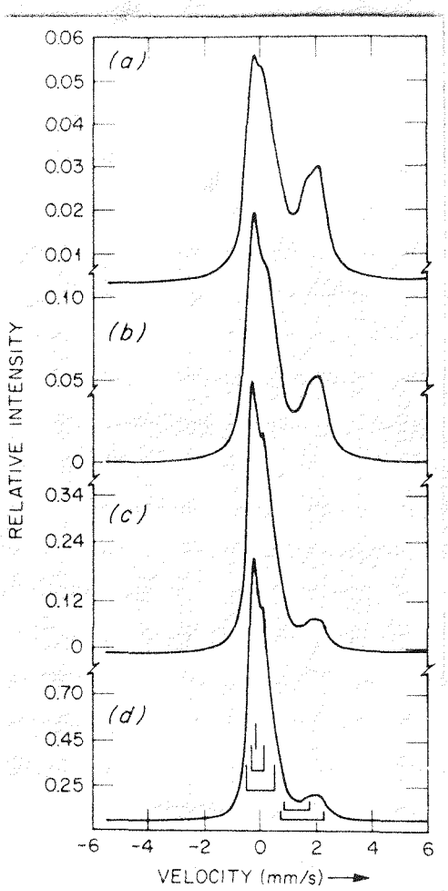

Fig. 5. CEMS spectra measured at 300 K for Al_2O_3 implanted with ^{57}Fe (160 keV, 77 K) to fluences of (a) 1 x 10^{16} ions/cm^2; (b) 2 x 10^{16} ions/cm^2; (c) 7 x 10^{16} ions/cm^2; (d) 1 x 10^{17} ions/cm^2.

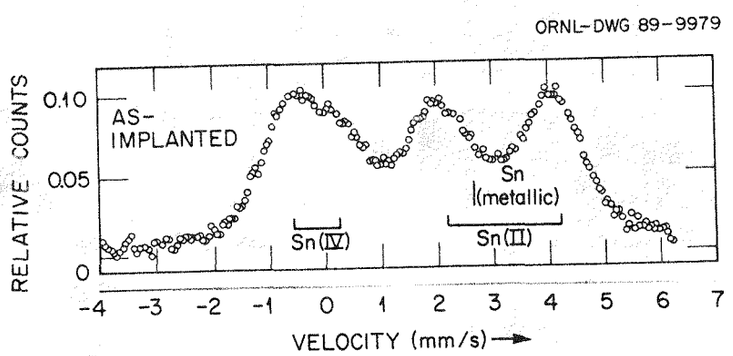

Fig. 6. CEMS spectra measured at 300 K for Al_2O_3 implanted with 4 x 10^{16} Sn/cm^2 (180 keV, 300 K).

oxygen ions with the Sn-O distances being greater in the direction perpendicular to the basal plane than in the basal plane. Likewise, a model for amorphous tin oxide consists of distorted oxygen octahedra containing central Sn^{4+} linked by Sn-O bonds with bridging Sn^{2+} on the apex of a pyramid [10]. As discussed above, Fe^{4+} occurs in complex compounds where the iron is contained in an elongated (FeO_6) octahedron.

SUMMARY

The amorphization of α-Al_2O_3 by implantation of Zr or Sn at room temperature suggests that a "chemical effect" in addition to displacement damage is responsible for this phase transformation. Data obtained by AEM measurements suggests that the critical concentration of Zr for amorphization is Zr/Al = 0.065 ± 0.01. Short-range order in amorphous Al_2O_3 has been measured and found to be implantation species-dependent. The chemical state (residual charge state) for Fe ions in amorphous Al_2O_3 is significantly different from that in crystalline α-Al_2O_3 matrices. Much of the iron the the amorphous phase exists in a Fe^{4+} state. Tin in amorphous Al_2O_3 exists in the states Sn(II) and Sn(IV).

ACKNOWLEDGEMENTS

This work was sponsored by the Divsiion of materials Sciences, U.S. Department of Energy, under contract DE-AC05-84OR21400 with Martin Marietta Energy Systems, Inc.

REFERENCES

1. G. C. Farlow, P. S. Sklad, C. W. White, C. J. McHargue, and B. R. Appleton, in Defect Properties and Processing of High Technology Nonmetallic Materials, edited by Y. Chen, W. D. Kingerly, and R. J. Stokes (Mater. Res. Soc. Proc. 60, Pittsburgh, PA 1986) pp. 387-394.

2. C. J. McHargue, G. C. Farlow, C. W. White, J. M. Williams, B. R. Appleton, and H. Naramoto, Mater. Sci. Engr. 69, 123 (1985).

3. P. S. Sklad, P. Angelini, and J. Sevely, in Proceedings of 46th Annual Meeting of the Electron Microscopy Soc. of America, edited by G. W. Bailey (San Francisco Press, San Francisco, CA, 1988) pp. 468-9.

4. C. J. McHargue, P. S. Sklad, J. C. McCallum, C. W. White, A. Perez, and G. Marest, to be published in Nucl. Instrum. Methods in Phys. Res. B.

5. C. J. McHargue, P. S. Sklad, J. C. McCallum, C. W. White, A. Perez, E. Abonneau, and G. Marest, to be published in Nucl. Instrum. Methods in Phys. Res. B.

6. N. N. Greenwood and T. C. Gibb, in Mössbauer Spectroscopy (Chapman and Hall, London, 1971) p. 249.

7. C. J. McHargue, G. C. Farlow, P. S. Sklad, C. W. White, A. Perez, N. Kornilios, and G. Marest, Nucl. Instrum. Methods in Phys. Res. B19/20, 813 (1987).

8. M. J. Rossiter, J. Phys. Chem. Sol. 26, 775 (1965).

9. G. Demazeau, B. Buffat, M. Pouchard, and P. Hagenmuller, J. Sol. State Chem. 54, 389 (1984).

10. C. S. Collins, T. Kachnowski, N. Benczer-Koller, and M. Pasternak, Phys. Rev. B19, 1369 (1979).